PUBLISHED VERSION

http://hdl.handle.net/2440/38972

Corrections to facilitate planar imaging of particle concentration in particle-laden flows using Mie scattering. Part 2: Diverging laser sheets

Peter A. M. Kalt* and Graham J. Nathan

School of Mechanical Engineering, University of Adelaide, Adelaide SA 5005, Australia

*Corresponding author: pkalt@mecheng.adelaide.edu.au

Part 1 describes a model to account for the effect of particles on laser sheet attenuation in flows where particles are heterogeneously distributed and where particles are small compared with the imaged volume. Here we extend the model to account for the effect of a strongly diverging light sheet, which is desirable when investigating many turbulent flows, e.g., in two-phase combustion problems. A calibration constant, C_κ, is derived to account for the attenuation of the incident laser sheet due to extinction of the laser beam through a seeded medium. This is shown to be effective in correcting both the effect of in-plane laser sheet attenuation and out-of-plane signal trapping due to particles in a jet flow heavily seeded with 5 g/s of 25–40 μm spherical particles. In the uncorrected case, attenuation causes up to 15% error in the mean concentration and 35% error on the rms fluctuations. Selecting an appropriate C_κ was found to remove the error in the mean concentration and reduce error on the rms fluctuation by half. Methods to estimate or measure an appropriate value of C_κ are also presented.   © 2007 Optical Society of America

OCIS codes: 290.5850, 100.2000, 110.2970.

1. Introduction

Most solid fuels, both of fossil or biomass origin, are burned in pulverized form, since this allows a greater combustion intensity than is possible with systems employing large particles, such as grate combustors. In pulverized combustion systems, the fuel is typically crushed to particle sizes of less than 100 μm. This allows them to be conveyed pneumatically and also provides a high surface-area-to-volume ratio for rapid combustion. Such particles are typically conveyed in the dilute phase, i.e., at velocities sufficient to prevent particles from settling to the floor of the duct, with mass loadings of less than 10 $\mathrm{kg_{particles}/kg_{air}}$ [1]. Under these conditions the volume fraction of particles is typically approaching 1%, and the number of particles is very large. It is difficult to measure particle numbers accurately under these conditions, since the size distribution is wide and total numbers are very sensitive to the large numbers of very fine

particles (<1 μm). Nevertheless, by way of illustration, a typical coal of density 1300 $\mathrm{kg/m^3}$ and a mass loading ratio of 10 would have more than 2×10^{12} particles per cubic meter, were all particles to be 10 μm in diameter. It should be noted that this mass loading typically represents the upper end of number density in combustion systems, since many systems would operate with somewhat lower mass loadings, and also the particles disperse as they move from the conveying system into, and through, the flame. Nevertheless, under conditions of relevance to pulverized fuel combustion, the effects of optical attenuation are very significant. This was noted by Smith *et al.* [2], for example, who performed imaging of the laser scattering from pulverized coal particles in a 2 MW, pilot-scale combustor. They were only able to obtain qualitative imaging largely because of the effects of attenuation. Nevertheless, the attenuation was not so great that the beam did not penetrate through the entire flame. This suggests that corrections may be possible under conditions of relevance to pulverized fuel combustion.

Knowledge of the instantaneous distribution and number density of coal particles as they disperse into a combustion chamber is important in the optimization of such systems. In the combustion of coal, for example, the instantaneous concentration has a direct influence to the ignition location, temperature, and emission production [3]. Public awareness of the detrimental effects of combustion emissions and government policies are driving the further optimization of coal combustion [4], and the use of replacement fuels, such as biomass and waste fuels [5]. However, industrial combustion systems are so complex that they can only be understood and optimized by the use of models. Such models require good quality data, both for their development and validation, obtained in simplified and well-defined environments. Knowledge of the number density and location of particles in such environments is hence an important component in the optimization of pulverized fuel combustion systems.

Research into solid fuel combustion of coal particles shows that phenomena such as clustering and roping have a major effect on global burning rates and other combustion properties [6]. It is therefore important to better understand and quantify the physics controlling roping. The formulation of theories is hampered by a lack of actual physical data. Clearly, instantaneously resolved planar concentration measurements of two-phase flows are important in addressing this need, but such imaging methods are difficult to implement successfully in a densely seeded two-phase flow.

One of the prime reasons driving the development of an instantaneous, planar nephelometry technique is to measure the large scale, heterogeneous distributions of particles on a shot-by-shot basis. To measure such distributions, in flows large enough to be representative of industrial scale two-phase flow issues, even the laboratory-scaled geometries are so large that a diverging laser sheet is a practical necessity. Most two-phase flows of practical interest also have seeding levels sufficiently high for the laser sheet to suffer significant attenuation by the second phase. This is commonly called *laser sheet extinction*. Also, the signal from the laser sheet may likewise be scattered as it is imaged by the collection optics. This is known as *signal trapping*. Both divergence and laser sheet extinction affect the local power of the illumination source and accordingly affect the signal of any concentration measurements made at that location. Out-of-plane scattering effects causing signal trapping are hard to account for because the location of the out-of-plane scattering bodies is resolvable only in the mean and rms sense, rather than instantaneously.

In-plane distributions of lightly seeded particles can be measured using the planar nephelometry method [7]. These planar imaging approaches extended the early work of Becker *et al.* [8] where turbulence statistics of a flow were inferred from the Mie-scattering signal of particles used as tracers. Kalt *et al.* [9,10] have developed an approach to correct for the effects of extinction in a parallel light sheet. The present study aims to extend the formulation of the *obscuration by particles* model [9,10] to a diverging laser sheet.

2. Obscuration of a Divergent Source by Particles

A. Extinction Model for a Diverging Laser Source

The light source considered for the *planar nephelometry* technique is a laser beam that is collimated in one axis and diverging in the perpendicular axis to form a laser sheet, as in Fig. 1. This arrangement is common in laser diagnostics. The laser sheet thickness remains nominally constant over the whole sheet, although it is often weakly focused in this plane by a long focal length lens. The divergence in the other plane allows large regions of space to be illuminated with the use of readily available optics.

The case of a diverging source is an extension of the collimated light sheet case, with many similarities. In both cases the particles are assumed to cast shadows without diffraction effects, similar to a ray-tracing model. A particle will obscure the laser sheet depending on its projected area in the direction of the light, which for small, spherical particles is the cross-sectional area. The transparent fraction, $\Gamma = 1 - A_p/A_{sheet}$, is the ratio of light in the laser sheet that is transmitted past a single-scattering body (particle). For a given size of particle its *shadow* in a diverging laser sheet will stretch along the divergent axis as shown schematically in Fig. 1. The stretching of the particle shadow in the divergent axis corresponds to an equivalent stretching of the laser sheets area as it diverges down beam.

The transparent fraction in a diverging laser sheet is thus a function of the down-beam location of the
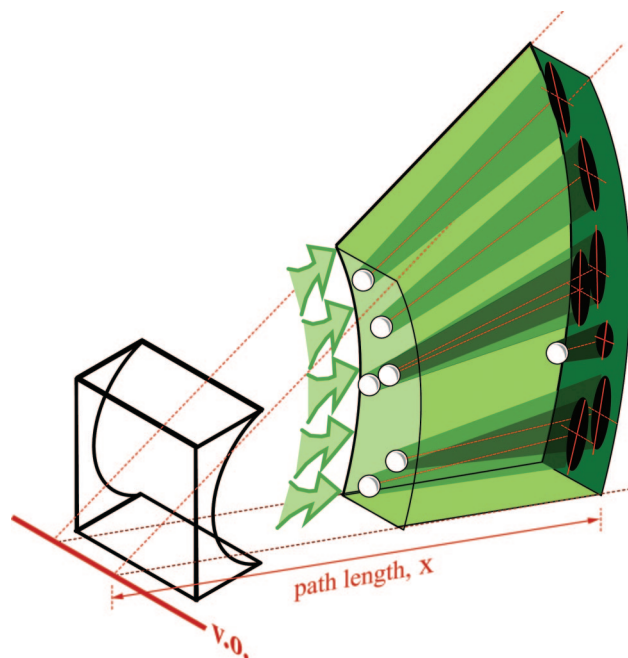

Fig. 1. (Color online) Schematic showing ray-trace model for diverging laser sheet of fixed thickness.
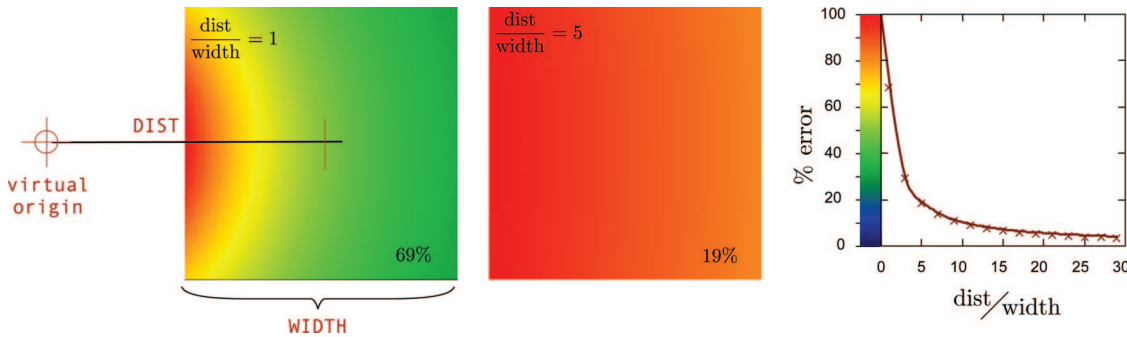
Fig. 2. (Color online) Magnitude of divergence errors based on relative position of virtual origin.

particle, x, and so is given the notation $\Gamma(x)$. Even though the particle cross section remains the same, it is a decreasing fraction of an ever-increasing divergent sheet, i.e.,

$$\Gamma(x) = (1 - \pi r_p^2 / A_{\text{laser}}(x)), \quad (1)$$

where r_p is the radius of the particle and $A_{\text{laser}}(x)$ is the local area of the laser sheet adjusted for divergence over a path length, x. That is, particles closer to the divergent source scatter a larger fraction of the available light, since the area of the sheet at that location is smaller than at locations further downbeam.

The *transmittance* along a ray interacting with many such scattering bodies is the product of the transparent fractions for all the scattering bodies up to that point, expressed as

$$\frac{I_1}{I_0} = \prod_{i=0}^{n_p} \Gamma(x). \quad (2)$$

Here n_p is the number of particles along the path, and $\Gamma(x)$ is determined for each particle.

B. Laser Fluence

There is another significant effect of divergence that needs to be taken into account, namely, the laser fluence. The laser fluence, or energy density, is a measure of the energy per unit area (J/m^2) over the laser sheet. The fluence decreases in the down-beam direction since the total energy within the laser sheet is constant, but the energy is spread out over a larger area as the beam diverges.

In the case of a *collimated* beam, the laser fluence does not change with down-beam distance. In the case of a laser sheet that diverges in one axis only, the fluence changes with the circumference of an arc, and so is inversely proportional to the distance to the virtual origin. For example, doubling the distance from the virtual origin will double circumference of the arc, doubling $A_{\text{laser}}(x)$, and halving the laser fluence at that location. The amount of energy scattered by a particle will be proportional to the local fluence, and so variation in the fluence needs to be accounted for over the imaged region, in order to normalize the scattered signal.

When the virtual origin is close to the imaging plane (dist/width = 1), divergence is a major influence on

local fluence, and variations in laser energy density can be as much as 69% over an image. See Fig. 2. When the virtual origin is far away, (dist/width $\gg$ 10) then the effect of divergence approaches other experimental uncertainties ($\sim$5%). More often than not, limits to lenses or available space will force a compromise when selecting a beam length.

C. Raster Imaging Plane

In digital planar imaging methods, data are recorded by a CCD detector. If the CCD comprises an $n \times m$ array of square pixels in the imaged plane, each pixel corresponds to an in-plane resolution in the object plane of ($\partial x = \partial y = R$ μm/pixel), and the imaged region is $nR \times mR$ μm². Figure 3(a) shows the imaged region, located within the laser sheet. This digital representation is known as a *raster*, whose origin is defined to be the top-left corner of the image.

The correction for attenuation needs to be implemented for the rasterized images. The volume of space imaged by each pixel has the shape of an extruded prism, with a height and width (∂x and ∂y) corresponding to the in-plane resolution of the camera, and a depth (∂z) equivalent to the thickness of the laser sheet. This is shown schematically in Fig. 3(b).

It is important to consider that the direction of the light is not always orthogonal to the raster orientation in the image. The angle θ is the average amount of misalignment between the raster orientation and the actual beam over a given pixel. The present corrections are derived for diverging cases where the orientation of the laser sheet is not always aligned to the raster plane and changes orientation depending on position in the imaged region. For a nonorthogonal beam path, it is possible to build a new, virtual beam path, made up of interpolated pixel values, shown schematically in Fig. 4. This beam path of interpolated pixels follows the direction of the ray from any given pixel back toward the the virtual origin of the laser source.

This simplification is very useful because if the image is looped on a pixel-by-pixel basis in a down-beam direction (i.e., columnwise rather than row-wise), starting at the edge closest to the laser source, then the extinction history at each pixel can be interpolated from the values of pixels already determined on previous iterations through the control loop.
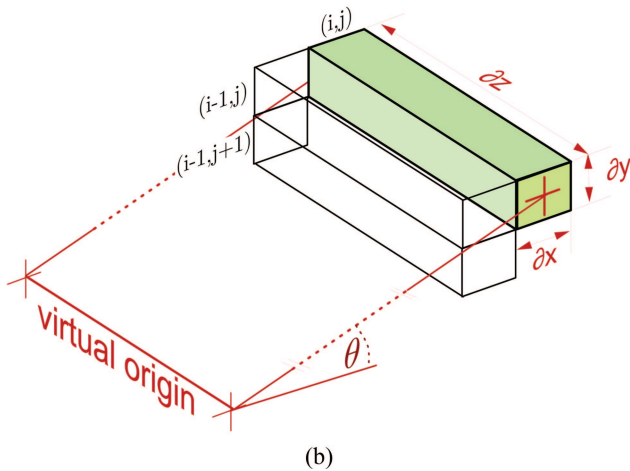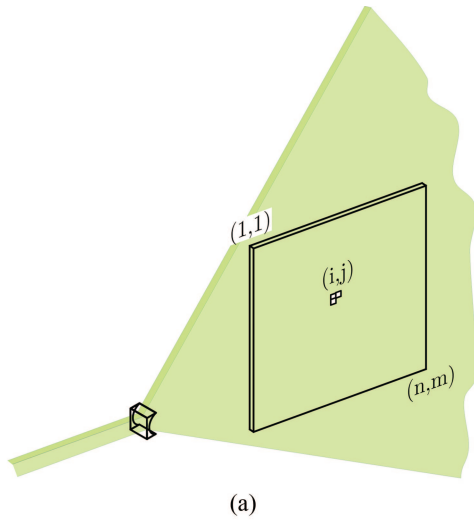
Fig. 3. (Color online) (a) Imaged plane of an $n \times m$ CCD, (b) imaged pixel volume, δx and δy are in-plane resolution, δz is laser sheet thickness.

D. Signal from a Pixel

The value registered within a pixel has many contributions, which may be characterized as either background, noise or signal. Removal of background, and estimable sources of noise are a first-order correction
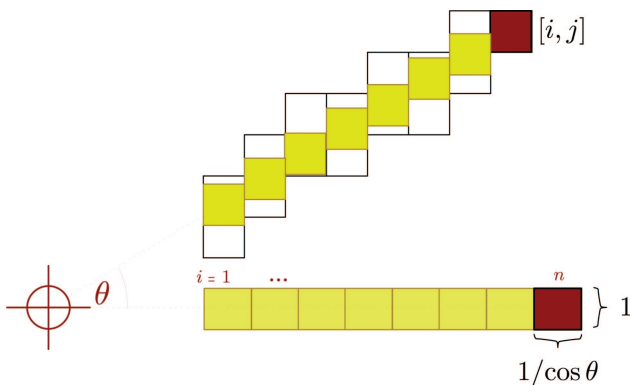

Fig. 4. (Color online) Beam path between virtual origin and pixel $[i, j]$ as a one-dimensional array of interpolated pixel values.

typically applied in image processing. The signal in the case of nephelometry is the Mie scattering from particles within the pixel volume. Each particle will scatter in many directions the light that it intercepts, which can be calculated from the product of the area of the particle and the local fluence.

When the scattered signal from the object plane is expressed in terms of rastered pixel volumes, the signal of a pixel located at $[i, j]$ is

$$\Phi[i, j] = C_\kappa \left(\overline{\pi r_p^2} \right) n_p[i, j] I'[i, j]. \tag{3}$$

For clarity, subsequent references to a quantity that varies spatially across an image omit the indices of the raster plane pixel position $[i, j]$ and denote the quantity with a tilde. Equation (3) may then be more succinctly expressed

$$\tilde{\mathbf{\Phi}} = C_\kappa \left(\overline{\pi r_p^2} \right) \cdot \tilde{\mathbf{n}}_p \cdot \tilde{I}'. \tag{4}$$

In Eq. (4), $\tilde{\mathbf{n}}_p$ is the number of particles in the pixel, $\tilde{I}'$ is the incident laser fluence entering the pixel. The term C_κ is a scaling constant representative of the efficiency in collecting the scattering. This includes terms such as the Mie-scattering cross section of the particles, the optical efficiency of the detector, and detector gain.

It should be noted that in some imaging applications the optical efficiency of the collector may not be the same over the whole of the imaged region. This would certainly be true in the case of large aperture (low f number) optics, where the center of the image is much brighter than the edges of the image which will suffer attenuation known as *vignetting*. In such cases, C_κ would be a quantity that varies over the imaged region and so would be noted $\tilde{C}_\kappa$. A useful, first-order estimate of the variation of $\tilde{C}_\kappa$ over an image could be achieved by the quantitative imaging of a uniform, diffuse light source in the imaging plane.

E. Polydisperse Particle Distributions

It is seldom the case in two-phase flows that the particles making up the solid phase are of a consistent size. More often than not, a particle sample is characterized by a distribution of sizes. Since it is rarely possible (or even advantageous) to image individual particles it is not possible to determine if a pixel has a high signal because it contains one large particle or several smaller ones.

Depending the laser sheet thickness, size of particles, mass loading of particles, etc., it is not uncommon to have tens or hundreds of particles imaged within a single pixel. Under this regime Eq. (3) is valid because

$$\pi r_1^2 + \pi r_2^2 + \cdots + \pi r_{n_p}^2 \approx \left(\overline{\pi r_p^2} \right) n_p = \frac{\pi}{4} d_{p(2,0)}^2 n_p. \tag{5}$$

Here $\overline{\pi r_p^2}$ is the average surface area, and $d_{p(2,0)}$ is the diameter based on equivalent surface area.

At sufficiently high volume loadings it is possible to use Eq. (3) reliably, if *local* size distribution is known. In this study the size distribution is assumed to be constant throughout the flow. This might not be the case, for example, in regions of a flow where the Stokes number of the larger particles is $\gg 1$ and that of the smaller particles is $\ll 1$. In such a flow, it would be advantageous to characterize the spatial variation of the distribution and apply that in Eq. (3). That is beyond the scope of the present paper. Nevertheless, in regions where the distribution is relatively constant, reliable data can be expected.

F. Correcting the Laser Fluence

Using Eq. (4), the effects of attenuation and divergence will serve to reduce the light present in the pixel volume, resulting in a value of $\tilde{I}'$ lower than the original, incident light, I_0.

$$\tilde{I}' = I_0 \times (\tilde{\kappa}_{\mathrm{div}} \times \tilde{\kappa}_{\mathrm{trans}} \times \tilde{\kappa}_{\mathrm{prof}} \times \cdots). \tag{6}$$

Corrections to the signal due to divergence, transmittance, and profile are implemented as normalization (gain) images, which adjust the incident light down to the appropriate local value. The determination of these variation normalization corrections is detailed in Subsections 2.G and 2.H.

G. Raster Implementation of Laser Fluence Correction

Figure 5 provides a schematic of light moving through a pixel volume. If $\tilde{I}'$ is the incident light entering a given pixel through the up-beam (y–z) surface, then the amount of light leaving a pixel through the opposite face is reduced by the inverse of the distance to the virtual origin. This does not violate the principle of conservation of energy since light also leaves through the normal faces in the x–z plane. The ratio
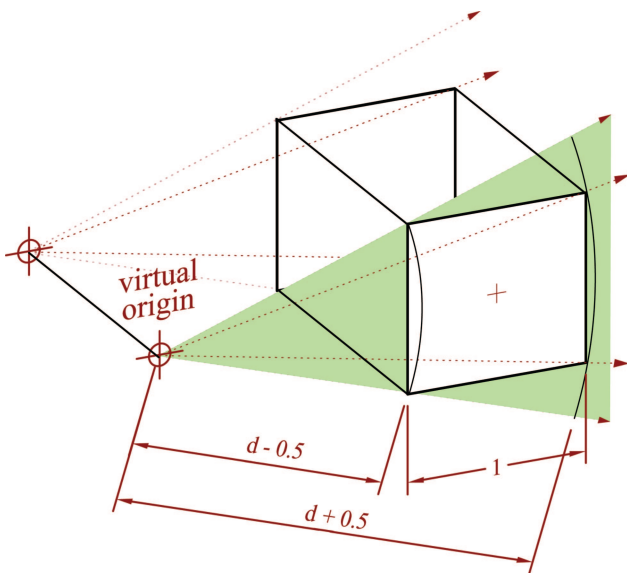

Fig. 5. (Color online) Schematic of diverging light passing through a pixel volume.

of these values is equal to our divergence normalization constant,

$$\tilde{\kappa}_{\mathrm{div}} = \tilde{I}_{\mathrm{out}}' / \tilde{I}_{\mathrm{in}}' = \frac{(d - 1/2)}{(d + 1/2)}, \tag{7}$$

Here, d is simply the distance from the pixel to the virtual origin (expressed in pixels). As the distance to the virtual origin increases, the beam becomes increasingly collimated and $\tilde{\kappa}_{\mathrm{div}} \to 1$. The normalization constant, $\tilde{\kappa}_{\mathrm{div}}$ is determined for each imaged pixel based on its position, as depicted in Fig. 2.

Considering the effects of divergence alone, along the one-dimensional beam of interpolated pixel values, the local laser intensity at the nth element, $\tilde{I}_n'$, is expressed as a ratio to the incident light, I_0,

$$\tilde{I}_n' = \left(\prod_{i=1}^{n} \kappa_{\mathrm{div}}[i] \right) I_0 \tag{8}$$

$$= \kappa_{\mathrm{div}}[n] \tilde{I}_{n-1}'. \tag{9}$$

H. Roster Implementation of Attenuation

Corrections for attenuation are readily implemented on a per pixel basis under the raster-based formulation. The amount of light unaffected by particle absorption and scattering in each pixel volume is the transmittance across that pixel volume,

$$\tilde{\kappa}_{\mathrm{trans}} = \left(1 - \frac{\overline{\pi r_p^2}}{\partial x \partial z \, \cos \theta} \right)^{\tilde{n}_p}, \tag{10}$$

where the laser sheet area is now replaced by the beam-normal surface area of the pixel volume ($= \partial x \partial z \cos \theta$). The absorption coefficient, $\tilde{\kappa}_{\mathrm{trans}}$, represents the fraction of the light entering a pixel volume able to pass through to illuminate down-beam pixels. This allows the attenuation normalization image, $\tilde{\kappa}_{\mathrm{trans}}$ to be generated in a single pass, rather than by iterating to convergence.

When considering the effects of attenuation by particles along a collimated one-dimensisonal beam, the local laser intensity at the nth element is expressed as

$$\tilde{I}_n' = \left(\prod_{i=1}^{n} \Gamma^{n_p[i]} \right) I_0 \tag{11}$$

$$= \kappa_{\mathrm{trans}}[n] \tilde{I}_{n-1}'. \tag{12}$$

Expressed more simply, if the proportion of light transmitted across the nth pixel is $\tilde{\kappa}_{\mathrm{trans}}[n]$, then the extinction history of the beam is equal to the product of all transmittances along the beam up to the nth element.

To find the transmittance of any given element, $\tilde{\kappa}_{\mathrm{trans}}[i]$, the number of particles in that pixel must be determined. This can be found from the measured signal at that element, $\tilde{\Phi}[i]$, and Eq. (4), provided that the scattering coefficient, C_κ, is known or can be estimated. It is then possible to combine the effects of

extinction and divergence along the whole of the beam by recursion, using a value of $\tilde{I}_{n-1}{}'$ interpolated from adjacent pixels in a marching fashion. It is assumed that the contribution to extinction within any single individual pixel is small, and so the light intensity across the pixel [I' in Eq. (4)] is approximately equivalent to the amount of light *entering* the pixel, namely, $\tilde{I}_{n-1}{}'$.

3. Validation Methodologies

A. Laser and Optics

The optical and imaging arrangement is shown in Fig. 6. A vertically polarized Nd:YAG laser, frequency doubled to 532 nm and pulsed at 10 Hz, was used as the source of illumination. The laser sheet was formed directly from the laser output beam, which was passed through a telescope of two cylindrical lenses to form a laser sheet of uniform 2 mm thickness. This reduced sheet was finally passed through a strong negative cylindrical lens [focal length (f.l.) −25 mm] to form a large sheet. The sheet diverges from a virtual origin located 25 mm upbeam of the final cylindrical lens. The position of the virtual origin is required to apply the attenuation corrections, traced back toward the source. Smoke images and shadows were recorded to identify the virtual origin.

B. Imaging Optics

Light was collected by a Kodak MegaPlus CCD, of 1008×1018 pixels and 10 bit resolution, with each exposure triggered by the laser flashlamp. The CCD was aligned orthogonal to the incident laser sheet. The overall imaging area was 200 mm × 200 mm. The region of interest was a subregion of t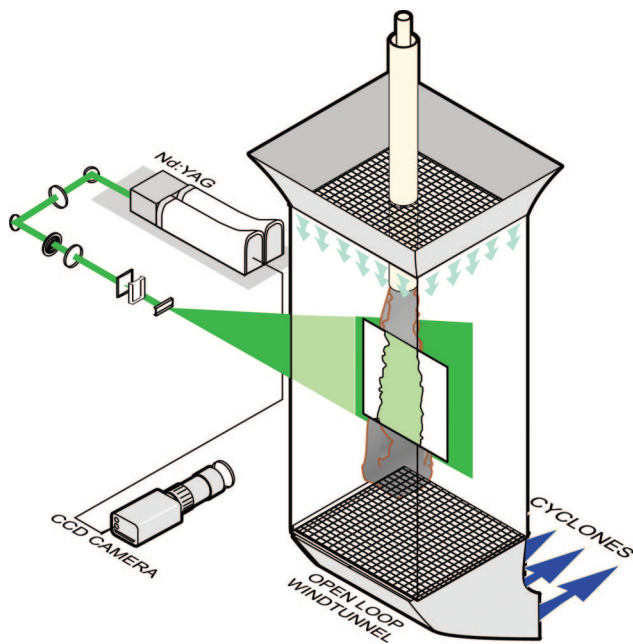he entire image, and the data ensemble was cropped down to a region 444 pixels wide by 950 pixels high. The location of the virtual origin was [−2113, 865], which makes dist/width ≈ 5. A Tamron 35–70 lens with aperture at f number 2.5 was used to image the laser sheet onto the CCD. Incident light was attenuated using a pair of cross-polarized filters, with one vertical and the other at a nonparallel alignment. The ensemble comprised 200 images.

C. Vertical Wind Tunnel

Experiments were conducted in an open-loop wind tunnel with a 650 mm × 650 mm square cross section, shown in Fig. 6. The tunnel is vertically orientated to avoid gravitational bias. A bell-mouth inlet and flow-conditioning screens provide a coflow with steady and uniform velocity of approximately 8 m/s. More details are provided by Birzer *et al.* [11,12].

D. Nozzle Arrangement and Geometry

Experiments and equipment were designed to simulate the preignition region of a typical rotary cement kiln. A coannular nozzle arrangement, similar to Fan *et al.* [13] and others [12] was investigated. It consists of a 50 mm diameter central jet, surrounded by an annulus [inner diameter (I.D.) = 60 mm, outer diameter (O.D.) = 70 mm]. In this arrangement the fuel (in this case the solid particles analogous to pulverized coal) is conveyed at 5 g/s in the annulus. The Reynold's number of the annulus was 39400, with a bulk velocity of 17 m/s. The central jet of air, without particles, is ordinarily used to drive mixing of the solid fuel and control the combustion characteristics. In this case, the central jet is not operated (bulk exit velocity of 0 m/s) and serves to act as a bluff body, encouraging the formation of a bluff body stabilized recirculation zone located at the exit plane of the nozzle. The development length of the central and annular nozzles was in excess of 100 diameters to avoid bias and allow fully developed initial flow. Great care was taken to ensure that the distribution of particles in the annulus and the exit velocity around the annulus are both symmetrical.

E. Solid Particles

Coal particles were simulated using Q-Cel hollow glass spheres with a size distribution shown in Fig. 7 and a density of approximately 700 kg/m^3. A Malvern particle sizer was used to characterize the diameters of the particle sample. The mean diameter of the distribution based on equivalent surface area, $d_{p(2,0)}$ is ∼21 μm. These provide equivalent Stokes number to 75 μm coal particles in a 35 MW, 3 m diameter cement kiln. Particles were introduced into the annular stream using a fluidized bed feeder. Mass loadings were determined by the change in mass of the feeder, as measured by a load cell and recorded on a computer. The mass flow rate of particles was moderately high at 5 g/s. For this mass loading and the pixel volume used in this experiment, the number of particles within a pixel volume ranged from 0 particles to over 100 particles in the near-field region at
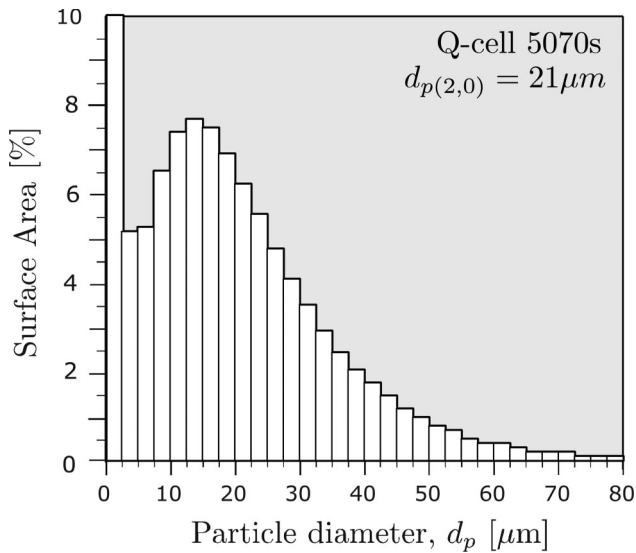

Fig. 6. (Color online) Two-phase wind tunnel setup including lasers and optics.

Fig. 7. Size distribution of Q-cell hollow glass particles used for validation.
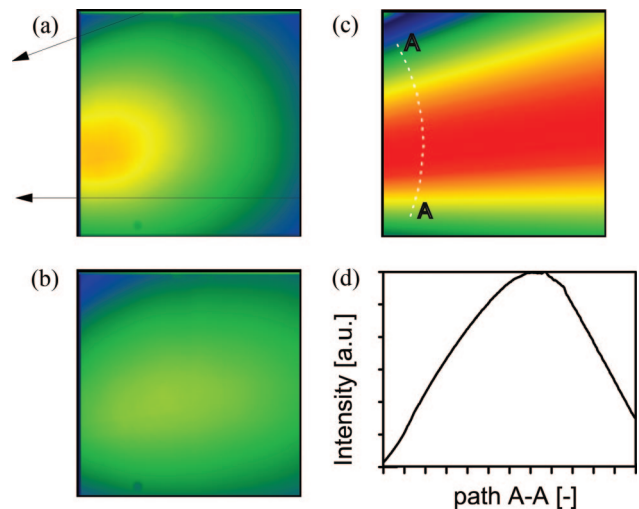

Fig. 8. (Color online) Corrections for profile: (a) Smoke image with location of virtual origin shown, (b) smoke image corrected for attenuation and divergence, (c) smoothed laser sheet profile response, and (d) plot of laser intensity along arc A–A.

the jet exit. At downstream locations, the number of particles per pixel was typically ∼10–20.

F. Laser Profile Corrections

The laser profile correction is *independent* of the divergence, attenuation, background or such corrections. The laser profile correction only accounts for the distribution of power (fluence) through the laser beam as generated by the laser. This will depend on whether a Gaussian or top-hat power profile is generated by the laser, depending on the mode of the laser. Using an aperture to trim away the low-power edges of the beam can also make the power through the laser beam more uniform. The exact corrections are therefore application specific.

In this study, the beam has a Gaussian distribution of power, which is then spread into a (diverging) laser sheet. The power drops off markedly toward the edges of the beam. An aperture is used to trim the beam edges.

The laser profile correction is therefore the first correction that is usually applied in laser diagnostics to normalize for variations in laser power within the beam itself. In planar laser induced fluorescence, for example, the beam profile is often measured shot to shot to enable calibration and quantification of the signal [14].

The best way to determine the beam profile is by direct measurement. This involves estimating the laser power distributed in the beam by imaging a uniform distribution of scattering bodies. In this case, a uniform smoke field (1 μm fog particles from a smoke generator) filled the vertical wind tunnel. Imaging this flat signal will not immediately give the laser profile correction, however, since the image will show the effects of divergence, attenuation, collection efficiency of the optics, variation of C_κ over an image, etc.

Carefully correcting the smoke image to remove the overlapping effects of divergence, attenuation,

and optics will leave a very good estimate of the laser power distributed in the laser sheet. Given that the optics are not altered between this profile calibration and the actual "nephelometry/data" measurements, the attenuation parameters are the same as the main experiment, except that the particle size is now only 1 μm instead of 25–40 μm.

Corrections for laser profile generated from smoke are shown in Fig. 8. Figure 8(a) shows the imaged smoke image as collected by the camera, including the effects of optics, attenuation, and laser fluence. Figure 8(b) shows the same image once corrected for the influence of attenuation and laser fluence. A slight *vignetting* at the edges of the imaged region can still be seen, suggesting that C_κ is not completely uniform over the imaged region. Figure 8(c) shows the smoke image corrected for all influences from optics and divergence. This is now equivalent to an image of $\tilde{\kappa}_{prof}$ and can be applied as the laser profile correction for fluence in Eq. (6). The path A–A indicated in Fig. 8(c) is a constant distance from the virtual origin. The intensity along this path is approximately Gaussian and corresponds to the Gaussian distribution of energy in the collimated leaser beam output from the single-mode laser. The smoke images were also used to find the location of the virtual origin relative to the imaged region, as described in Subsection 3.A.

4. Validation Results

A. Instantaneous Corrections

The instantaneous images were first processed to remove background signal. This includes contributions from the CCD dark charge as well as the secondary reflections from optics in the absence of particles. A typical instantaneous image, corrected for background, is shown in Fig. 9(a).
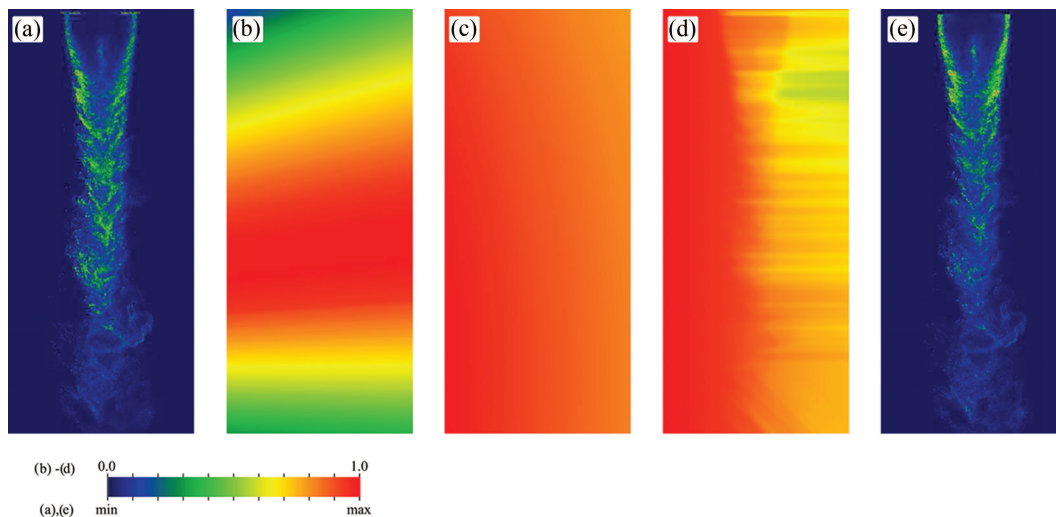
Fig. 9. (Color online) Instantaneous image corrections: (a) Original instantaneous Mie image, (b) laser sheet profile (response), (c) divergence (with virtual origin at [−2118, 865]), (d) transmittance ($C_\kappa = 1.5$), and (e) corrected instantaneous image.

The laser sheet exhibits a Gaussian power distribution through the laser beam, as is typical for a single-mode Nd:YAG laser. Normalizing by the intensity distribution corrects for the differences in local laser sheet power due to the Gaussian beam profile. The profile, determined from corrected flat-field smoke images is shown in Fig. 9(b). Here, the variation in power is ~50% over the imaging region, which represents a correction larger than that of the divergence and attenuation combined.

Figure 9(c) shows the divergence correction given the position of the virtual origin (here [−2113, 865] pixels with respect to the origin at the top left of the image). The magnitude of divergence effect is significantly less than 20% for most of the image, given that the image is 444 pixels wide, and dist/width ≈ 5.

The corrections for attenuation have been determined on a shot-by-shot basis from the instantaneous images. Figure 9(d) presents the attenuation normalization for the instantaneous image shown in Fig. 9(a). For the current data set, $C_\kappa = 1.5$ was determined by symmetry of the mean signal to account for a bias of 35% in the uncorrected mean particle concentration image.

Figures 9(b)–9(d) show the response images to account for the effect of varying laser intensity due to laser profile, divergence, and attenuation. Dividing the detected signal by these responses will normalize the resulting signal to account for losses in illumination. These may be applied, in any order, to give a (semiquantitative) corrected instantaneous image of particle concentration, shown in Fig. 9(e).

B. Determination of C_κ

A range of strategies can be employed to determine the appropriate value of C_κ if the experiment is appropriately designed to facilitate that process. For instance, it is possible to place a reflective polymer strip in the down-beam edge of the imaging region, to provide a strip image proportional to the laser power

per unit area along the laser sheet height. Normalizing the shot-to-shot signal from this strip will give an instantaneous record of the local transmittance. A single value of C_κ can be selected that will duplicate the attenuation behavior.

Alternately, a C_κ can be selected to remove eccentricities in the ensemble mean image of a symmetrical flow. This can be used when the magnitude of attenuation is sufficiently small. In such cases, the biases due to attenuation are often only clearly visible in the mean and rms images of particle concentration. If the flow is known to be symmetrical around the axis, then C_κ can be selected to remove the bias in the ensemble mean image, as in Fig. 10(a). The rms image is particularly sensitive to small fluctuating quantities. Selecting C_κ to remove bias in the ensemble mean also drastically improves the resolved rms, as shown in Fig. 10(b). Figure 11 shows radial profiles of average and rms intensity taken through the *neck* region of the coannular flow, which is indicated in Fig. 10 by a dashed line. Corrected ($C_\kappa = 1.5$) and uncorrected profiles at this downstream location are shown. Increasing C_κ will increase the relative contribution of the attenuation corrections, until the actual losses on the mean due to attenuation are matched. The bias on the rms of particle concentration drops from over 32% to ~16%.

5. Discussion

For the current experiments with 5 g/s mass flow rate of particles, which was sufficiently high for the laser sheet to be attenuated by up to 40% through the flow. The greatest attenuation (~40%) was found to occur in the near-field neck region, near the end of the recirculation zone. The presence of the neck zone is wholly expected, and this causes the particle density there to be the highest of anywhere in the flow. Further downstream, the effect of attenuation is significantly lower, typically 5%–10% of the sheet. Nevertheless, this is still the same order of
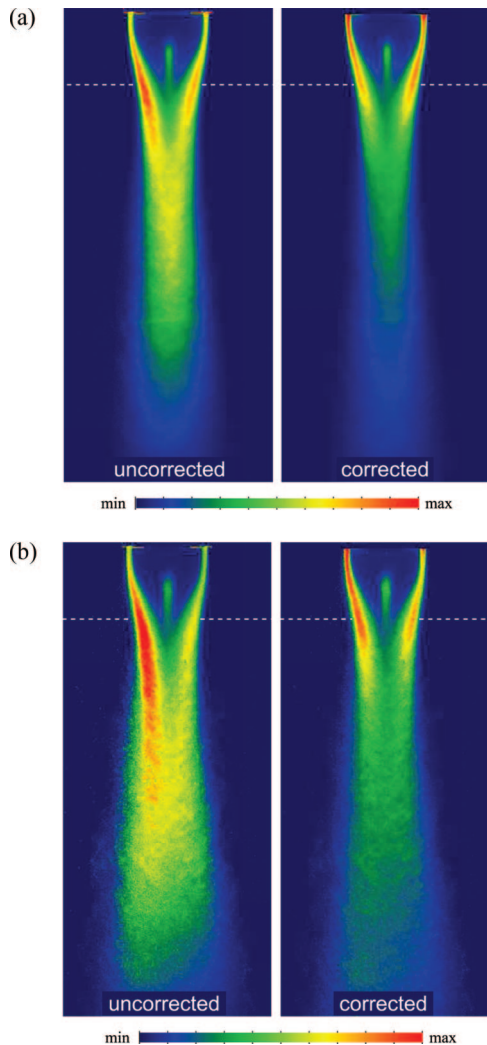
Fig. 10. (Color online) Effect of corrections of ensemble statistics for $C_\kappa = 1.5$: (a) mean images, (b) rms variance image. Dashed line indicates the location of profiles shown in Fig. 11.

Fig. 11. (Color online) Effect of attenuation corrections on signal profiles through the neck region indicated in Fig. 10: (a) mean, (b) rms.

magnitude as the effect of divergence throughout the imaged region.

The value of C_κ will determine the derived number of particles inferred from the measured signal. It is important to note that the correction is not strongly sensitive to an accurate measure of C_κ. For example, an error in C_κ by 50% results in a 9%–12% error in the corrected signal, down from ~30% when uncorrected. Hence, even a useful *estimate* will improve the accuracy considerably.

It is also worth recalling that the present corrections were applied with a polydisperse size distribution typical of many practical multiphase flows. It is also applied in an annular flow with quite high velocity gradients. That useful corrections were still obtained under these conditions demonstrates the utility of the method. Further accuracy may be possible were the method to be extended to also measure the local size distribution, such as by the laser sheet dropsizing method of Jermy and Greenhalgh [15] or phase-Doppler analysis.
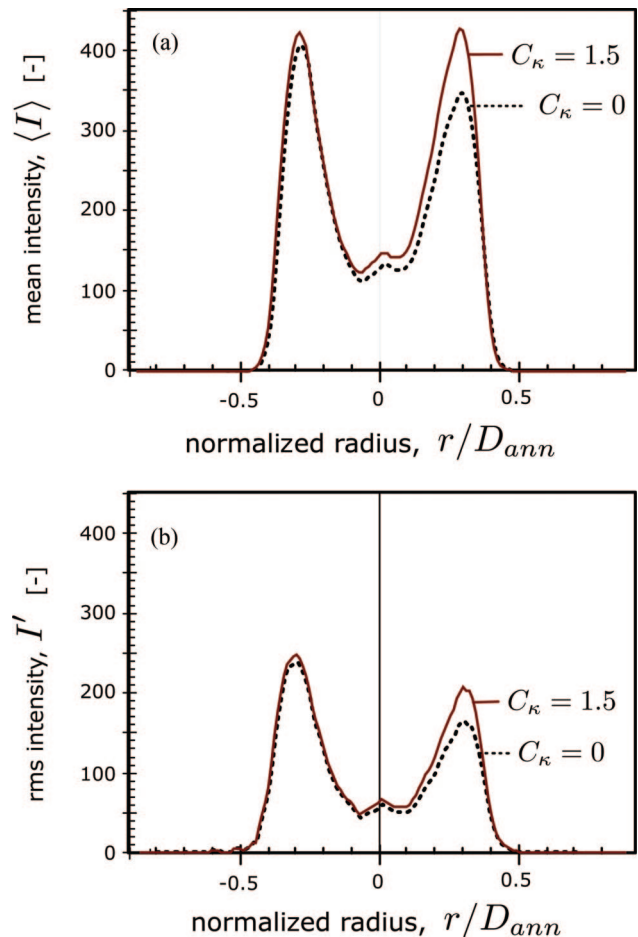
6. Conclusions

A model to correct for extinction of light by a high mass loading of particles has been developed for a monochromatic laser sheet that diverges in one axis, used to illuminate a densely seeded two phase flow. The model accounts for the effects of divergence and extinction of the laser beam due to scattering by particles. It is applicable where the particles are large relative to the wavelength of light but small compared with the volume imaged by each pixel.

The extinction model is able to correct for both divergence and laser sheet extinction due to high mass loading. When applied to a validation data set, the appropriate selection of the scaling parameter C_κ enables biases in the resolved mean and rms to be reduced or removed entirely by correcting the instantaneous images on a shot-by-shot basis. Biases in the mean flow of the validation data set were found to be entirely removed, down from approximately 30% at the high mass loading case (5 g/s). Biases in the rms were found to be reduced from 32% to 15% in the neck region where attenuation effects are most pronounced. The corrections are demonstrated to be relatively insensitive to C_κ, even when mass loading is so high as to result in a transmittance of only 70%

(i.e., an attenuation of 30%) and for a polydisperse particle distribution. Even a crude estimate of C_κ serves to reduce errors on the mean from 30% down to 9%–12%, given moderately high particle loading that results in serious attenuation errors.

The value of C_κ, necessary for optimizing the corrections, can be determined using several strategies. The most accurate is to measure directly the instantaneous laser sheet extinction through the image. This allows C_κ to be obtained on an instantaneous basis, i.e., for each shot in the ensemble. Also of high accuracy is the iterative approach to determine C_κ in a way that removes measured asymmetries or biases in the mean and rms ensembles. However, this requires the flow to be known to be symmetrical *a priori*. Finally, as a last resort, in the case where corrections are to be applied to previously collected data with suspected flow biases, C_κ can be estimated from similar imaging conditions. Provided that laser sheet extinction is less than ~30%–40%, a reasonable estimate of C_κ will reduce, rather than exacerbate, the magnitude of errors due to laser sheet extinction.

References

1. S. Dhodapkar, L. Bates, G. Klinzing, and P. Wypych, "Guidelines for solids storage, feeding and convening," Chem. Eng. **113,** 26–33 (2006).
2. N. L. Smith, G. J. Nathan, D. K. Zhang, and D. S. Nobes, "The significance of particle clustering in pulversied coal flames," Proc. Combust. Inst. **29,** 797–804 (2002).
3. H. M. Cassel and I. Leibman, "The cooperative mechanism in the ignition of dust dispersions," Combust. Flame **3,** 467–472 (1959).
4. W. Fulkerson, R. R. Judkins, and M. K. Sanghvi, "Energy from fossil fuels," Sci. Am. (September 1990), pp. 83–89.
5. L. L. Baxter, L. Ip, and K. Cen, "Distinguishing biomass combustion characteristics and their implications for sustainable energy," in *5th Asia-Pacific Conference on Combustion,* G. J. Nathan, B. B. Dally, and P. A. M. Kalt, eds. (The Combustion Institute, 2005), pp. 496–474.
6. N. L. Smith, "The influence of the spectrum of jet turbulence on the stability, NO_x emissions and heat release profile of pulverised coal flames," Ph.D. dissertation (Department of Mechanical Engineering, University of Adelaide, 2000).
7. C. H. Birzer, P. A. M. Kalt, G. J. Nathan, and N. L. Smith, "The influence of mass loading on particle distribution in the near field of a co-annular jet," in *15th Australasian Fluid Mechanics Conference* (The University of Adelaide, 2004), pp. AFMC00205.
8. H. A. Becker, H. C. Hottel, and G. C. Williams, "On the light-scatter technique for the study of turbulence and mixing," J. Fluid Mech. **30,** 259–284 (1967).
9. P. A. M. Kalt and C. H. Birzer, "Calibrations for planar nephelometry in densely seeded two-phase flows," in *Fourth Australian Conference on Laser Diagnostics in Fluid Mechanics and Combustion,* Z. T. Alwahabi, B. B. Dally, P. A. M. Kalt, G. J. Nathan, and C. Y. Wong, eds. (University of Adelaide, 2005).
10. P. A. M. Kalt, C. H. Birzer, and G. J. Nathan, "Corrections to facilitate planar imaging of particle concentration in particle-laden flows using Mie-scattering, Part 1: Collimated laser sheets," Appl. Opt. **46,** 5823–5834 (2007).
11. C. H. Birzer, P. A. M. Kalt, G. J. Nathan, and N. L. Smith, "Planar measurements of the distribution of particles in a two-phase precessing jet flow," in *Proceedings of the 5th Asia-Pacific Conference on Combustion,* B. B. Dally, G. J. Nathan, and P. A. M. Kalt, eds. (The Combustion Institute, 2005), pp. 105–108.
12. C. H. Birzer, P. A. M. Kalt, and G. J. Nathan, "The influence of particle mass-loading on mean particle distributions in the near field of a co-annular jet," Int. J. of Multiphase Flows (to be published).
13. J. Fan, H. Zhao, and K. Cen, "An experimental study of two-phase turbulent coaxial jets," Exp. Fluids **13,** 279–287 (1992).
14. P. R. Medwell, P. A. M. Kalt, and B. B. Dally, "Simultaneous imaging of OH, formaldehyde, and temperature of turbulent nonpremixed jet flames in a heated and diluted coflow," Combust. Flame **148,** 48–61 (2007).
15. M. C. Jermy and D. A. Greenhalgh, "Planar dropsizing by elastic and fluorescence scattering in sprays too dense for phase doppler measurement," Appl. Phys. B, **71,** 703–710 (2000).